# Linear and circular dichroism in photoelectron angular distributions caused by electron correlation

Yoshi-Ichi Suzuki and Toshinori Suzuki*
*Department of Chemistry, Graduate School of Science, Kyoto University, Kitashirakawa-Oiwakecho, Sakyo-Ku, Kyoto 606-8502, Japan*
(Received 2 August 2014; published 18 May 2015)

Electron correlation can break the symmetry of photoelectron angular distribution upon two-step ionization to a doubly degenerate ionic state via a doubly degenerate intermediate state. The interference between the two components of the intermediate state prepared using linearly and circularly polarized light is discussed for cyclopropane as an example.

DOI: 10.1103/PhysRevA.91.053413 PACS number(s): 33.80.Rv, 33.60.+q, 82.53.Kp

Although electron correlation plays a crucial role in chemical reactions and bonding [1,2], it is difficult to identify experimentally. Correlation energy, defined as the difference between the true energy and the Hartree-Fock energy, cannot be measured because the latter is a theoretical value estimated by neglecting the electron correlation. On the other hand, the occurrence of some electronic transitions, such as the satellite bands [3–5] and non-Koopmans transitions [6] observed with photoelectron spectroscopy, manifests the breakdown of independent electron approximation due to the electron correlation. Photoionization differential cross sections may exhibit more details of the electron correlation; for example, two photoelectrons in double photoionization [7] have been simultaneously detected to examine the correlation between two electrons. However, is it always a requirement to observe two or more electrons to identify electron correlation? It is noted that the violation of Kepler's second law is identified by observing a single planet; therefore, it should be possible to identify the electron correlation by the observation of a single electron in photoionization. The aim of this study is to explore the possibility to detect electron correlation clearly by the observation of single photoionization.

The theory of photoelectron angular distributions for atoms and molecules has been developed for many decades [8–18]. However, most applications of these theories have dealt with nondegenerate electronic states, which is one reason why the independent electron theory can often predict photoelectron angular distributions very well. In this study, we consider a two-step ionization in the perturbation regime as shown in Fig. 1(a) via a doubly degenerate state to a doubly degenerate cation state. Let us specify the symmetry of the neutral and cation states, respectively, by the irreducible representations (irreps) $\Gamma$ and $\Gamma_+$, where

$$|\Gamma\rangle + h\nu \rightarrow |\Gamma_+\rangle + e^-. \tag{1}$$

The point group of the neutral and cation states is assumed to be the same [19,20]. The symmetry of the ionized (Dyson) orbital $\gamma_t$ [21] must be contained in the direct product $\Gamma \otimes \Gamma_+$.

As an example, we consider the photoionization of cyclopropane ($C_3H_6$) via the $3s$ ($1\,^1E'$) and $3p$ ($2\,^1E'$) Rydberg states to the ground ($^2E'$) state of the cation [22,23]. Cyclopropane belongs to the $D_{3h}$ point group [Fig. 1(b)]. The $3s$ and $3p$ Rydberg states are mixed because they belong to the same irrep via the electron-electron interaction. For those states, $\gamma_t$ can be $a_1'$, $a_2'$, and $e'$ (i.e., $E' \otimes E'$), whereas within the single configuration approximation, the $\gamma_t$ of the $3s$ and $3p$ Rydberg states, respectively, are $a_1'$ and $e'$ alone. Therefore, the observables that are described by the interference between $\gamma_t$ and $\gamma_t'$ $(\neq \gamma_t)$ indicate mixing of the configuration. The contribution of $a_2'$ symmetry is small [22], which is probably ascribed to the $a_2'$ symmetry appearing as an $f$ or higher angular momentum state. Here we consider only the electron correlation for bound states [1,2] so that interchannel coupling [24] is not included. The strong orthogonality [25,26] between continuum orbitals and a bound state wave function is assumed to be preserved.

A general form of photoelectron angular distribution is given by

$$I(\theta,\varphi) = \sum_{L\geqslant 0} \sum_{|M_L|\leqslant L} B_{LM_L} Y_{LM_L}(\theta,\varphi), \tag{2}$$

where $Y_{LM_L}(\theta,\varphi)$ represents the spherical harmonics. The $B_{LM_L}$ coefficients are dependent on the molecular state, light polarization, and photoionization dynamics [27]. $B_{LM_L}$ may be zero, depending on whether the electron correlation is taken into account or not. This is clearly different from other observables, which manifest the electron correlation effects as deviations from the expected values using the independent electron approximation. In the following discussion, we consider the two cases of a molecule fixed in space and an isotropically distributed molecular ensemble (Table I).

The $B_{LM_L}$ coefficients can be calculated from the wave function of an $N$-electron eigenstate $|\Gamma q\rangle$ belonging to an irrep $\Gamma$ and its component $q$. $|\Gamma q\rangle$ may be expanded approximately with $(N-1)$-electron states $|\Gamma_+ q_+\rangle$ and one-electron states $|\gamma_t q_t\rangle$. $(\Gamma_+,q_+)$ and $(\gamma_t,q_t)$ are the pairs of an irrep and its component for the final cation state and the Dyson orbital, respectively,

$$|\Gamma q\rangle = \sum_{\gamma_t\in\Gamma\otimes\Gamma_+} c_{\gamma_t} \sum_{q_+,q_t} |\Gamma_+ q_+\rangle |\gamma_t q_t\rangle \langle \Gamma_+ q_+ \gamma_t q_t | \Gamma q\rangle, \tag{3}$$

where $\langle \Gamma_+ q_+ \gamma_t q_t | \Gamma q\rangle$ represent the Clebsch-Gordan coefficients [10,21,28]. The Dyson orbitals are defined as

$$\langle \boldsymbol{r} | \Gamma_+ q_+; \Gamma q\rangle = \sum_{\gamma_t q_t} c_{\gamma_t} \langle \boldsymbol{r} | \gamma_t q_t\rangle \langle \Gamma_+ q_+ \gamma_t q_t | \Gamma q\rangle, \tag{4}$$

where $\boldsymbol{r}$ represents the spatial coordinates of an electron. This equation is used to extract the $c_{\gamma_t}$ coefficients from the Dyson orbitals. For a short probe pulse with a bandwidth larger than

*suzuki@kuchem.kyoto-u.ac.jp

 

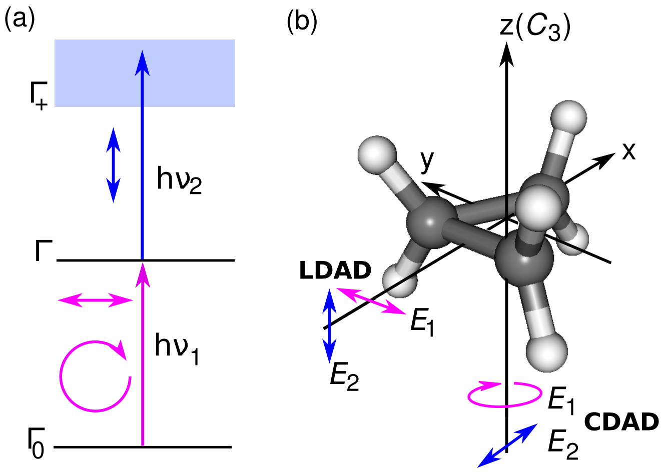


FIG. 1. (Color online) (a) Two-step ionization scheme from the ground state $\Gamma_0$ to a cation state $\Gamma_+$ via an intermediate state $\Gamma$. The polarization of light for the excitation is linear or circular, whereas linearly polarized light is assumed for the ionization. (b) A cyclopropane molecule with molecular frame axes. The $z$ axis is parallel to the threefold symmetry axis ($C_3$). Typical polarizations of light for the first and second steps, respectively, are shown by arrows $E_1$ and $E_2$. LDAD and CDAD represent linear and circular dichroisms in the photoelectron angular distributions, respectively.

the rotational envelope of an ionization transition, the $B_{LM_L}$ coefficients are expressed as

$$B_{LM_L} = \sum_{q_+}\sum_{qq'}\sum_{\gamma_t q_t}\sum_{\gamma_t' q_t'}\sum_{KQ\Lambda p}\sum_{k_2 q_2}(-1)^{L-M_L} \times c_{\gamma_t} c_{\gamma_t'} \langle \Gamma_+ q_+ \gamma_t q_t | \Gamma q\rangle \langle \Gamma_+ q_+ \gamma_t' q_t' | \Gamma q'\rangle^* \times \begin{pmatrix} K & L & k_2 \\ Q & -M_L & q_2 \end{pmatrix} \rho^{(\nu_2)}_{k_2 q_2} A^{(q,q')}_{KQ\Lambda p} b^{(\gamma_t q_t,\gamma_t' q_t')}_{KLk_2\Lambda p}, \quad (5)$$

where $\rho^{(\nu_2)}_{k_2 q_2}$ is the state multipole of the ionization laser light [18]. $A^{(q,q')}_{KQ\Lambda p}$'s describe the molecular axes alignment and the polarization of a degenerate electronic state. $b^{(\gamma_t q_t,\gamma_t' q_t')}_{KLk_2\Lambda p}$'s represent the generalized anisotropy parameters that are dependent on the photoionization transition dipole moments and reflect the symmetry selection rules [18,29,30].

For fixed-in-space molecules, two types of phenomena are identified in which the specific $B_{LM_L}$'s shown in Table I are ascribed to electron correlation. These $B_{LM_L}$'s cause symmetry breaking of the photoelectron angular distributions. The patterns of symmetry breaking differ with the light polarization so that these phenomena are distinguished as LDAD and CDAD. Typical polarizations of light are shown in Fig. 1(b).

For freely rotating molecules, most of the $B_{LM_L}$'s are zero, whereas the exception is Im[$B_{2\pm2}$] for the CDAD. The derivation of $B_{LM_L}$'s shown in Table I is given in the Appendices.

The physical origin of $B_{LM_L}$'s in Table I is the mixing of different symmetry (irreps) in the generalized anisotropy parameters $b^{(\gamma_t q_t,\gamma_t' q_t')}_{KLk_2\Lambda p}$, i.e., $(a_1',e')$ and $(a_2',e')$ for the LDAD and $(a_1',a_2')$ for the CDAD (Table I). These pairs are related to the electron correlation, whereas the mixing of $(e_x',e_y')$ for the CDAD (Table I) is not related. It is noted that the pairs of irreps in such an interference are different between the LDAD and the CDAD. Thus, the LDAD and CDAD provide complementary information on electron correlation.

Let us compare the present two-step scheme for the CDAD and a conventional scheme for the CDAD [14,15,31]. In the present scheme, circularly polarized light is used for excitation and the intermediate state must be degenerate, whereas in the conventional CDAD scheme, circular polarization is used for ionization and the intermediate state can be nondegenerate. The CDADs in both schemes give rise to nonzero Im[$B_{2\pm2}$].

We now consider the case for cyclopropane. Calculations are performed for the $S_0$ equilibrium geometry optimized using the second-order Møller-Plesset perturbation theory with the cc-pVDZ basis set [32]. One-electron wave functions are obtained using the state-average complete active space level calculations with the basis set augmented with a set of diffuse functions [22]. For continuum states, $S$-matrix normalized one-electron wave functions are obtained by continuum multiple scattering $X\alpha$ calculations [33,34]. These one-electron functions are used to construct single- and multiple-configuration wave functions, and then bound-continuum transition dipoles are obtained using the electric dipole approximation [35].

Figures 2(a) and 2(d) show the polarization and propagation directions of laser light for the two-step ionization with respect to the fixed-in-space molecule. Figures 2(b) and 2(e) show calculated photoelectron angular distributions for the $3p$ Rydberg state using a single-configuration wave function, whereas Figs. 2(c) and 2(f) show those using a multiple-configuration wave function. These figures illustrate the striking effects of electron correlation on photoelectron angular distribution. The threefold symmetry is preserved for the single-configuration wave function and is independent of the propagation direction of laser light. In contrast, the threefold symmetry is broken in the photoelectron angular distributions for the multiple-configuration wave function. The normalized coefficients Re[$B_{LM_L}$]/$B_{00}$ are as large as 0.17 and 0.08 for $(L,M_L) = (1,1)$ and (3,1), respectively, in Fig. 2(c). These asymmetries are sufficiently large to detect experimentally. It is noted that the $c_{\gamma_t}$ coefficients are independent of the photoelectron kinetic energy. Nevertheless, the degree of

TABLE I. Photoelectron anisotropy coefficients for LDAD and CDAD that are induced by the interference of orbitals $(\gamma_t,\gamma_t')$ in $D_{3h}$. $n$ and $n'$ are integers.

| | Fixed-in-space molecules | Isotropic ensemble of molecules | $(\gamma_t,\gamma_t')$ |
|---|---|---|---|
| LDAD | $B_{L,3n\pm1}$, $L+3n\pm1=2n'$ | | $(a_1',e')$,$(a_2',e')$ |
| CDAD | Im[$B_{LM_L}$], $L+M_L=2n'$ | Im[$B_{2,\pm2}$] | $(a_1',a_2')$,$(e_x',e_y')$ |

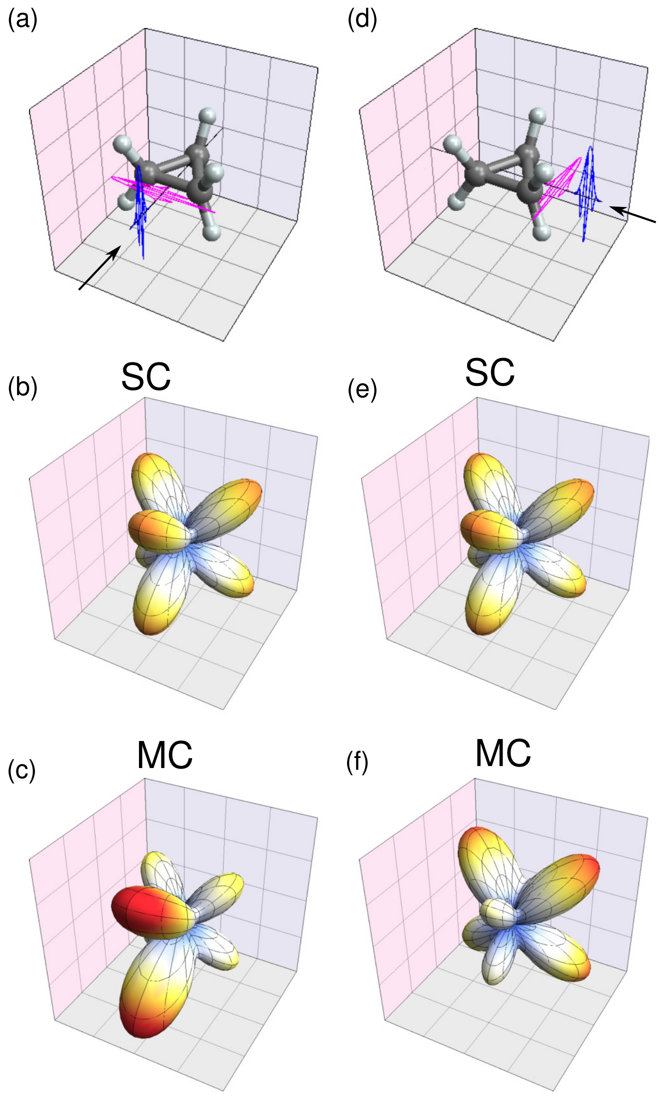


FIG. 2. (Color online) Linear dichroism in photoelectron angular distributions. (a) A cyclopropane molecule and two linearly polarized laser lights. The arrows indicate the propagation direction of the laser lights. The electric-field vector for the excitation (ionization) light is perpendicular (parallel) to the threefold symmetry axis. Molecular frame photoelectron angular distributions are calculated with (b) single-configuration (SC) and (c) multiple-configuration (MC) wave functions of the $3p$ Rydberg state at a photoelectron kinetic energy (PKE) of 0.1 eV. (d)–(f) are the same as (a)–(c), respectively, but with the different propagation direction of laser light. The photon energies are assumed to be 8.5 and 3.0 eV for $h\nu_1$ and $h\nu_2$, respectively.

symmetry breaking is dependent on the photoelectron kinetic energy (Fig. 3) because at least the Coulomb phases of electron partial waves vary with the energy [18].

In the case of photoexcitation of an isotropic ensemble of molecules, the alignment-polarization parameters generally become time dependent and are dependent on the initial rotational state distribution. To eliminate this complexity for the sake of the discussion, we assume that all molecules are initially in the rotational ground state. In this case, photoexcitation ($^1A_1' - {}^1E'$) produces two degenerate states ($N = 1, \kappa = \pm 1$), where $N$ and $\kappa$ denote the molecular angular momentum and its projection on the molecular $C_3$ symmetry axis. This assumption makes the axis alignment time independent.

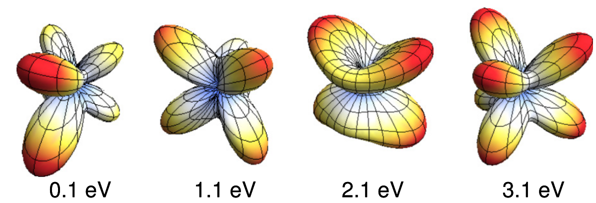


FIG. 3. (Color online) Photoelectron angular distributions for different photoelectron kinetic energies. The molecular and laser configurations are the same as Fig. 2(a), and the wave function is the multiple-configuration wave function of the $3p$ Rydberg state.

Figures 4(b) and 4(c) show the photoelectron angular distributions of the two-step ionization via the $3s$ and $3p$ Rydberg states, respectively. The $3s$ Rydberg state does not exhibit a CDAD in the single-configuration approximation as indicated by the red solid line in Fig. 4(b). The nonzero $\mathrm{Im}[B_{22}]$ in Fig. 4(b) arises from electron correlation (blue dashed line). In this example $\mathrm{Im}[B_{22}]$ is the largest at a photoelectron kinetic energy of 0.3 eV. However, $\mathrm{Im}[B_{22}]$ in Fig. 4(b) is extremely small because $a_2'$ orbitals play almost no role in this ionization: The coefficient of $c_{a_2'} = 0.012$ is much smaller than $c_{a_1'} = 0.977$ and $c_{e'} = 0.157$ for the $3s$ Rydberg state. In contrast, the photoelectron angular distribution of the $3p$ Rydberg state exhibits large left-right asymmetry due to interference between the $e_x'$ and the $e_y'$ components in Fig. 4(c).

The discussions can be extended with slight modifications to ionizations from the doubly degenerate to the doubly

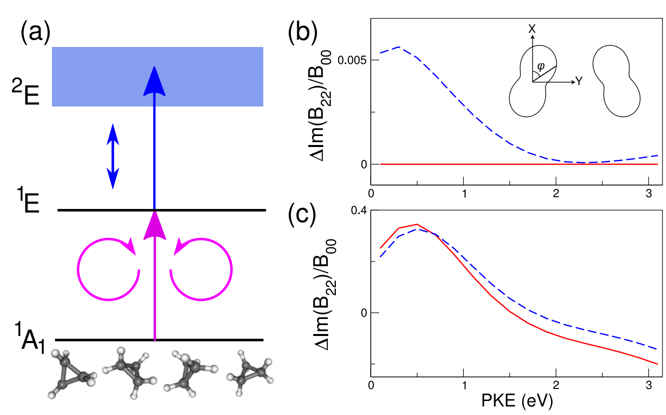


FIG. 4. (Color online) Circular dichroism in photoelectron angular distributions. (a) Excitation scheme for the randomly oriented molecular ensemble. Calculated difference of anisotropy parameter $\Delta\,\mathrm{Im}(B_{22})/B_{00} = \mathrm{Im}(B_{22}^{\mathrm{left}})/B_{00}^{\mathrm{left}} - \mathrm{Im}(B_{22}^{\mathrm{right}})/B_{00}^{\mathrm{right}}$ for the (b) $3s$ and (c) $3p$ Rydberg states as a function of the photoelectron kinetic energy. The solid and dashed lines indicate the results for single- and multiple-configuration wave functions, respectively. The inset of (b) defines the axes. The excitation laser light is circularly polarized and propagates along the laboratory $Z$ axis, whereas the ionization laser light is linearly polarized parallel to the $X$ axis and propagates in the same direction of excitation laser light. The photon energies of $h\nu_2$ are assumed to be $h\nu_2 = \mathrm{PKE} + \mathrm{IE} - h\nu_1$ eV, where IE is the ionization potential of cyclopropane 11.4 eV [23] and $h\nu_2$ are the excitation energies for the Rydberg states (7.9 and 8.5 eV for $3s$ and $3p$, respectively).

degenerate states of most point groups. For $C_{\infty v}$, however, there is no one-electron function that belongs to $\sigma^-$ ($a_2'$ in $D_{3h}$). Therefore, the CDAD cannot be used to examine the effect of electron correlation in the ${}^1\Pi$-${}^2\Pi$ ionization, for instance.

From an experimental perspective, the photoelectron angular distributions for the fixed-in-space molecules are difficult to observe, especially for polyatomic molecules. One possible solution would be molecular adsorption on a solid surface [36,37]. Although the wave functions for excited states would be substantially deformed upon adsorption, the symmetry-breaking phenomena can be observed assuming that the system, the surface, and a molecule have well-defined symmetry with degenerate states. Another solution would be to use the dissociative ionization for linear molecules and methyl halides [34,38] under the axial recoil approximation. Our preliminary calculations show that electron correlation can still cause the symmetry breaking of photoelectron angular distributions for such an axially averaged system.

To summarize, symmetry breaking in photoelectron angular distributions upon single photoionization can reveal electron correlation. As an example, our calculations indicate large asymmetry in the photoelectron angular distributions upon photoionization from a doubly degenerate $3p$ Rydberg state to a doubly degenerate cation state for a cyclopropane molecule fixed in space. The weak circular dichroism for the $3s$ Rydberg state reflects very weak mixing of $a_2'$ symmetry. The interference effects between the components that belong to different irreps can provide relative phase information for different electronic configurations, which is useful for experimental characterization and a deeper understanding of many-electron wave functions.

## ACKNOWLEDGMENTS

This work was supported by a Kakenhi Grant-in-Aid (Grant No. 25410010) from the Japan Society for the Promotion of Science and by the "X-ray Free Electron Laser Priority Strategy Program" of the Ministry of Education, Culture, Sports, Science and Technology, Japan.

## APPENDIX A: NONZERO $B_{LM_L}$ FOR CORRELATED WAVE FUNCTIONS

In this Appendix, we provide a detailed explanation for the $B_{LM_L}$ parameters in Table I. We first consider the excitation of a molecule fixed in space with either linearly or circularly polarized light in which the linearly polarized light propagates perpendicular to the $C_3$ axis, whereas the circularly polarized light propagates parallel with the $C_3$ axis. In these cases, the alignment-polarization parameters can be expressed as

$$A^{(q,q')}_{KQ\Lambda p} = A_{KQ\Lambda p}\mu^{(\nu_1)}_q \mu^{(\nu_1)*}_{q'}, \tag{A1}$$

where $A_{KQ\Lambda p}$ is an alignment parameter [18,29] and $\mu^{(\nu_1)}_q$ and $\mu^{(\nu_1)}_{q'}$ are the coefficients for the superposition of an intermediate state $\mu^{(\nu_1)}_x|E_x\rangle + \mu^{(\nu_1)}_y|E_y\rangle$, which are dependent on the light polarization for excitation. The sum over $q_+$, $q$, $q'$, $q_t$, and $q_t'$ in Eq. (5) can be performed using $\mu^{(\nu_1)}_q$ and $\mu^{(\nu_1)}_{q'}$ and the Clebsch-Gordan coefficients for $D_{3h}$.

For linearly polarized light, if the electron correlation is negligible, i.e., $\gamma_t = \gamma_t'$, then the sum over $q_+$, $q$, $q'$, $q_t$, and $q_t'$ results in an incoherent sum over $q_t$,

$$\begin{aligned}\sum_{q_+}\sum_{qq'}\sum_{q_tq_t'}&\langle\Gamma_+q_+\gamma_tq_t|\Gamma q\rangle\\ &\times\langle\Gamma_+q_+\gamma_tq_t'|\Gamma q'\rangle^* b^{(\gamma_tq_t\gamma_tq_t')}_{KLk_2\Lambda p}\mu^{(\nu_1)}_q\mu^{(\nu_1)*}_{q'}\\ &=\frac{1}{d}\left(\left|\mu^{(\nu_1)}_x\right|^2+\left|\mu^{(\nu_1)}_y\right|^2\right)\sum_{q_t} b^{(\gamma_tq_t\gamma_tq_t)}_{KLk_2\Lambda p},\end{aligned} \tag{A2}$$

where $\Gamma_+ = \Gamma = E'$, $d = 1$ for $\gamma_t = a_1'$ and $a_2'$ and $d = 2$ for $e'$. An incoherent sum over $q_t$ with equal weights in Eq. (A2) results in photoelectron angular distributions with threefold symmetry when the polarization of light for ionization is linear and parallel to the $C_3$ axis (the proof is provided in the next section). Hence, the $B_{LM_L}$ coefficients with $M_L = 3n \pm 1$ ($n$ is an integer) vanish when the electron correlation is negligible. On the other hand, the electron correlation gives rise to additional terms that contain $b^{(\gamma_tq_t,\gamma_t'q_t')}_{KLk\Lambda p}$ with $(\gamma_tq_t,\gamma_t'q_t')$ of $(a_1',e_x')$, $(a_2',e_y')$, $(a_1',e_y')$, and $(a_2',e_x')$. The threefold symmetry in the photoelectron angular distribution will then be broken by symmetry mixing of $(a_1',e')$ and $(a_2',e')$, which results in nonzero $B_{LM_L}$ of $M_L = 3n \pm 1$. The values of these $B_{LM_L}$'s are dependent on the polarization of the pump light. Thus, the electron correlation exhibits LDAD as shown in the second row of Table I.

For circularly polarized light and without electron correlation, a cross term of $e_x'$-$e_y'$, $\rho b^{(e_x',e_y')}_{KLk\Lambda p}$ is to be added to Eq. (A2) for $\gamma_t = e'$, whereas the sum is identical to Eq. (A2) for $\gamma_t = a_1'$ and $a_2'$. Here, $\rho$ is defined as $\mu^{(\nu_1)*}_x\mu^{(\nu_1)}_y - \mu^{(\nu_1)}_x\mu^{(\nu_1)*}_y$. An additional term $\rho b^{(a_1',a_2')}_{KLk\Lambda p}$ appears when electron correlation is strong. The terms depending on $\rho$ indicate the occurrence of CDAD [12,14,15,31] because the sign of the factor $\rho$ changes for the left and the right circularly polarized light. Im[$B_{LM_L}$]'s are not zero if the ionization laser light is linearly polarized and propagates parallel to the pump light along the $C_3$ axis. In addition, those generalized anisotropy parameters show that the circular dichroism is a result of mixing $(e_x',e_y')$ and $(a_1',a_2')$ (third row of Table I).

For freely rotating molecules, Eq. (A1) cannot be used. The alignment-polarization parameters are proportional to the state multipole of $\rho^{(\nu_1)}_{KQ}$ for the excitation laser light [39],

$$A^{(\nu_1,q,q')}_{KQ\Lambda p} = a^{(q,q')}_{K\Lambda p}\rho^{(\nu_1)}_{KQ}. \tag{A3}$$

The coefficients $a^{(q,q')}_{K\Lambda p}$ can be classified into one of the irreps of the "four" group by the parities of $K + p$ and $\Lambda$ [39] as ee, eo, oe, and oo. The circularly polarized light is described by the sign of $\rho^{(\nu_1)}_{10}$. There are three expansion coefficients $a^{(q,q')}_{100}$, $a^{(q,q')}_{110}$, and $a^{(q,q')}_{111}$ because $\Lambda$ and $p$ must be in the range of $0 \leqslant \Lambda \leqslant K$, $p = 0$ for $\Lambda = 0$ and $p = 0,1$ for $\Lambda > 0$. These three $a^{(q,q')}_{K\Lambda p}$ parameters are classified by $K + p$ and $\Lambda$ as oe, oo, and eo, respectively, but not the totally symmetric ee. Those $a^{(q,q')}_{K\Lambda p}$ can arise from the coherence of two rotational states created upon the $A_1' \to E'$ electronic transition, resulting in nonzero Im[$B_{2\pm2}$].

## APPENDIX B: A SYMMETRY PROPERTY OF $B_{LM}$

### 1. Selection rules for one-electron wave functions

We assume that $\phi_{e,x}(r,\theta,\varphi)$ and $\phi_{e,y}(r,\theta,\varphi)$ are the one-electron functions that belong to two-dimensional irreps $e$ for molecules with an $n$-fold symmetry axis. Because those two functions can be a basis set for the irreps $e$, they are mutually related by a rotation operator $\hat{C}_n$ as

$$\hat{C}_n\phi_{e,x}(\boldsymbol{r}) = \cos\varphi_n\phi_{e,x}(\boldsymbol{r}) - \sin\varphi_n\phi_{e,y}(\boldsymbol{r}),$$

where $\varphi_n = \frac{2\pi}{n}$ and $\boldsymbol{r} = (r,\theta,\varphi)$ are polar coordinates. The effect of $\hat{C}_n$ on the $S$-matrix normalized continuum wave function $\psi^{(-)}_{l\lambda}(\boldsymbol{r};E)$ [33] is a factor $e^{i\lambda\varphi_n}$ since the Hamiltonian commutes with $\hat{C}_n$ and the function changes by $\hat{C}_n$ from $Y_{l\lambda}(\theta,\varphi)$ to $Y_{l\lambda}(\theta,\varphi+\varphi_n)$ at the boundary ($r\to\infty$). $E$ is the photoelectron kinetic energy, and $Y_{l\lambda}(\theta,\varphi)$ is a spherical harmonics with angular momentum $l$ and its projection on the molecular $z$ axis $\lambda$,

$$\hat{C}_n\psi^{(-)}_{l\lambda}(\boldsymbol{r};E) = e^{i\lambda\varphi_n}\psi^{(-)}_{l\lambda}(\boldsymbol{r};E).$$

Therefore, we obtain a relation in transition dipole moments $I^{(\gamma_t q_t)}_{l\lambda s}(E)$,

$$\begin{aligned} I^{(e,x)}_{l\lambda s}(E) &= \hat{C}_n I^{(e,x)}_{l\lambda s}(E) = e^{i(s-\lambda)\varphi_n}\int \psi^{(-)*}_{l\lambda}(\boldsymbol{r};E)rY_{1s}(\theta,\varphi)[\cos\varphi_n\phi_{e,x}(\boldsymbol{r}) - \sin\varphi_n\phi_{e,y}(\boldsymbol{r})]d\boldsymbol{r} \\ &= e^{i(s-\lambda)\varphi_n}\big[\cos\varphi_n I^{(e,x)}_{l\lambda s}(E) - \sin\varphi_n I^{(e,y)}_{l\lambda s}(E)\big], \end{aligned}$$

and, hence,

$$I^{(e,y)}_{l\lambda s}(E) = \frac{e^{-i(s-\lambda)\varphi_n} - \cos\varphi_n}{-\sin\varphi_n} I^{(e,x)}_{l\lambda s}(E). \tag{B1}$$

Similarly, we obtain

$$I^{(e,y)}_{l\lambda s}(E) = \frac{e^{i(s-\lambda)\varphi_n} - \cos\varphi_n}{\sin\varphi_n} I^{(e,x)}_{l\lambda s}(E), \tag{B2}$$

using $\hat{C}_n^{-1}$. When $I^{(e,x)}_{l\lambda s} \neq 0$, the following relation must hold:

$$\frac{e^{-i(s-\lambda)\varphi_n} - \cos\varphi_n}{-\sin\varphi_n} = \frac{e^{i(s-\lambda)\varphi_n} - \cos\varphi_n}{\sin\varphi_n},$$

which can be simplified as

$$s - \lambda = nN \pm 1, \qquad N \in \text{integer}. \tag{B3}$$

For $n = 3$, those equations can be summarized as

$$I^{(e,y)}_{l\lambda s} = \begin{cases} 0, & s-\lambda = 3N, \\ i I^{(e,x)}_{l\lambda s}, & s-\lambda = 3N+1, \\ -i I^{(e,x)}_{l\lambda s}, & s-\lambda = 3N+2, \quad N \in \text{integer}. \end{cases} \tag{B4}$$

These relations hold for the irreps $e'$ and $e''$ of the $D_{3h}$ point group as well as $e$ of $C_{3v}$.

### 2. Symmetry of small $b$ parameters

The generalized anisotropy parameters [18,29] can be written as

$$\begin{aligned} b^{(\gamma_t q_t,\gamma_t' q_t')}_{KLk_2\Lambda p}(E) &= \sum_{ll'}\sum_{\lambda\lambda'}\sum_{ss'}\sqrt{3[l][l'][L][k_2]}\frac{(-1)^{1+s+\lambda'+K}}{\sqrt{2(1+\delta_{0\Lambda})}}\begin{pmatrix} l & l' & L \\ 0 & 0 & 0\end{pmatrix}\sum_{\Lambda_L\lambda_2}\left[\begin{pmatrix} L & K & k_\gamma \\ \Lambda_L & \Lambda & \lambda_\gamma\end{pmatrix} + (-1)^p\begin{pmatrix} L & K & k_2 \\ \Lambda_L & -\Lambda & \lambda_2\end{pmatrix}\right] \\ &\quad\times\begin{pmatrix} l & l' & L \\ \lambda & -\lambda' & \Lambda_L\end{pmatrix}\begin{pmatrix} 1 & 1 & k_2 \\ -s & s' & \lambda_2\end{pmatrix} J^{(\gamma_t q_t)}_{l\lambda s}(E) J^{(\gamma_t' q_t')*}_{l'\lambda' s'}(E), \end{aligned} \tag{B5}$$

where

$$J^{(\gamma_t q_t)}_{l\lambda s}(E) = i^{-l}e^{i\eta_l(E)}I^{(\gamma_t q_t)}_{l\lambda s}(E),$$

and $\eta_l(E)$ is the Coulomb phase. The essential part of the incoherent sum of $b^{(\gamma_t q_t,\gamma_t' q_t')}_{KLk_2\Lambda p}(E)$ over $q_t$ for $e'$ orbitals can be calculated using Eq. (B4),

$$J^{(e'x)}_{l\lambda s}(E)J^{(e'x)*}_{l'\lambda' s'}(E)+J^{(e'y)}_{l\lambda s}(E)J^{(e'y)*}_{l'\lambda' s'}(E)=\begin{cases}0, & s-\lambda=3n \text{ or } s'-\lambda'=3n' \\ & \text{or } (s-\lambda=3n\pm1 \text{ and} \\ & s'-\lambda'=3n'\mp1), \\ 2J^{(ex)}_{l\lambda s}(E)J^{(ex)*}_{l'\lambda' s'}(E), & s-\lambda=3n\pm1 \text{ and} \\ & s'-\lambda'=3n'\pm1,\end{cases} \tag{B6}$$

where $n$ and $n'$ are arbitrary integers. From the $3j$ symbols in Eq. (B5), $b^{(eq_t,eq_t)}_{KLk_2\Lambda p}(E)$ becomes zero unless

$$\Lambda=\pm(\Lambda_L+\lambda_2)=\pm(-\lambda+\lambda'+s-s'). \tag{B7}$$

Combining Eqs. (B6) and (B7), we have

$$\sum_{q_t} b^{(eq_t,eq_t)}_{KLk_2\Lambda p}(E)=0,\qquad \Lambda\neq 3n. \tag{B8}$$

Similarly, we can obtain

$$b^{(\gamma_t q_t,\gamma_t q_t)}_{KLk_2\Lambda p}(E)=0,\qquad \Lambda\neq 3n \tag{B9}$$

for $\gamma_t=a_1'$ or $a_2'$ from Eq. (B5) and $I^{(a_j')}_{l\lambda s}=0$ $(j=1,2)$ for $s-\lambda\neq 3N$.

### 3. Anisotropy parameters $B_{LM_L}$

In the single-configuration approximation, Eq. (5) can be written as

$$B_{LM_L}=\sum_{q_+}\sum_{q_t}\sum_{KQ}\sum_{k_2q_2}\sum_{\Lambda p}(-1)^{L-M_L}\begin{pmatrix}K & L & k_2\\ Q & -M_L & q_2\end{pmatrix}\rho^{(\nu_2)}_{k_2q_2}A_{KQ\Lambda p}\left(\left|\mu_x^{(\nu_1)}\right|^2+\left|\mu_y^{(\nu_2)}\right|^2\right)b^{(\gamma_t q_t,\gamma_t q_t)}_{KLk_2\Lambda p}(E),$$

where we used Eq. (A1). When the light polarization for ionization is linear and parallel to the $C_3$ axis, the $q_2$ of nonzero $\rho^{(\nu_2)}_{k_2q_2}$ is zero. For the molecules whose $xyz$ axes coincide the laboratory frame $XYZ$ axes [18,29], the alignment parameters are given by

$$A_{KQ\Lambda p}=\frac{2K+1}{8\pi^2}\frac{1}{\sqrt{2(1+\delta_{0\Lambda})}}[\delta_{Q\Lambda}+(-1)^p\delta_{Q,-\Lambda}].$$

Therefore, we obtain

$$B_{LM_L}=\sum_{q_+}\sum_{q_t}\sum_{KQ}\sum_{k_2}\sum_{\Lambda p}(-1)^{L-M_L}\begin{pmatrix}K & L & k_2\\ Q & -M_L & 0\end{pmatrix}\rho^{(\nu_2)}_{k_2,0}\frac{2K+1}{8\pi^2}\frac{1}{\sqrt{2(1+\delta_{0\Lambda})}}[\delta_{Q\Lambda}+(-1)^p\delta_{Q,-\Lambda}]$$
$$\times\left(\left|\mu_x^{(\nu_1)}\right|^2+\left|\mu_y^{(\nu_2)}\right|^2\right)b^{(\gamma_t q_t,\gamma_t q_t)}_{KLk_2\Lambda p}(E).$$

From this equation and Eqs. (B8) and (B9), we obtain that $B_{LM_L}$ is zero unless

$$M_L=Q=\pm\Lambda=\pm3n,$$

i.e., the photoelectron angular distribution has a threefold symmetry.


[1] A. Szabo and N. S. Ostlund, *Modern Quantum Chemistry: Introduction to Advanced Electronic Structure Theory* (Dover, New York, 1996).

[2] S. Wilson, *Electron Correlation in Molecules*, Dover Books on Chemistry (Dover, New York, 2007), p. 44.

[3] L. S. Cederbaum, W. Domcke, J. Schirmer, and W. von Niessen, Many-body effects in valence and core photoionization of molecules, Phys. Scr. **21**, 481 (1980).

[4] V. Schmidt, *Electron Spectrometry of Atoms Using Synchrotron Radiation*, Cambridge Monographs on Atomic, Molecular, and Chemical Physics (Cambridge University Press, Cambridge, UK, 1997).

[5] R. Wehlitz, B. Langer, N. Berrah, S. B. Whitfield, J. Viefhaus, and U Becker, Angular distributions of helium satellites $He^+nl$ ($n=2$–7), J. Phys. B: At., Mol. Opt. Phys. **26**, L783 (1993).

[6] T. Horio, T. Fuji, Y.-I. Suzuki, and T. Suzuki, Probing ultrafast internal conversion through conical intersection via time-energy map of photoelectron angular anisotropy, J. Am. Chem. Soc. **131**, 10392 (2009).

[7] J. S. Briggs and V. Schmidt, Differential cross sections for photo-double-ionization of the helium atom, J. Phys. B: At., Mol. Opt. Phys. **33**, R1 (2000).

[8] D. Dill, Resonances in photoelectron angular distributions, Phys. Rev. A **7**, 1976 (1973).

[9] V. L. Jacobs, Theory of atomic photoionization measurements, J. Phys. B: At. Mol. Phys. **5**, 2257 (1972).
[10] D. Dill and U. Fano, Parity unfavoredness and the distribution of photofragments, Phys. Rev. Lett. **29**, 1203 (1972).
[11] D. Dill, Fixed-molecule photoelectron angular distributions, J. Chem. Phys. **65**, 1130 (1976).
[12] B. Ritchie, Theory of the angular distribution of photoelectrons ejected from optically active molecules and molecular negative ions, Phys. Rev. A **13**, 1411 (1976).
[13] N. A. Cherepkov, Circular dichroism of molecules in the continuous absorption region, Chem. Phys. Lett. **87**, 344 (1982).
[14] R. L. Dubs, S. N. Dixit, and V. McKoy, Circular dichroism in photoelectron angular distributions from oriented linear molecules, Phys. Rev. Lett. **54**, 1249 (1985).
[15] N. A. Cherepkov, V. V. Kuznetsov, and V. A. Verbitskii, Photoionization of polarized atoms, J. Phys. B: At., Mol. Opt. Phys. **28**, 1221 (1995).
[16] S. Motoki, J. Adachi, K. Ito, K. Ishii, K. Soejima, A. Yagishita, S. K. Semenov, and N. A. Cherepkov, Complete photoionization experiment in the region of the $2\sigma_g \rightarrow \sigma_u$ shape resonance of the $N_2$ molecule, J. Phys. B: At., Mol. Opt. Phys. **35**, 3801 (2002).
[17] N. M. Kabachnik, S. Fritzsche, A. N. Grum-Grzhimailo, M. Meyer, and K. Ueda, Coherence and correlations in photoinduced auger and fluorescence cascades in atoms, Phys. Rep. **451**, 155 (2007).
[18] Y.-I. Suzuki and T. Suzuki, Determination of ionization dynamical parameters by time-resolved photoelectron imaging, Mol. Phys. **105**, 1675 (2007).
[19] We assumed that the laser band width is larger than the Jahn-Teller splittings, in order to preclude the possible effect of Jahn-Teller distortion on the symmetry of photoelectron angular distributions, although to our knowledge the effect is small [20].
[20] H. Shiromaru and S. Katsumata, Photoelectron angular distribution for Jahn-Teller split bands of some molecules in VUV photoelectron spectroscopy, Bull. Chem. Soc. Jpn **57**, 3453 (1984).
[21] The subscript $t$ of $\gamma_t$ stands for "transfer" because $\gamma_t$ is the transferred angular momentum for atomic photoionizations [10].
[22] E. Goldstein, S. Vijaya, and G. A. Segal, Theoretical study of the optical absorption and magnetic circular dichroism spectra of cyclopropane, J. Am. Chem. Soc. **102**, 6198 (1980).
[23] I. C. Walker, D. M. P. Holland, D. A. Shaw, I. J. McEwen, and M. F. Guest, The electronic states of cyclopropane studied by VUV absorption and ab initio multireference configuration interaction calculations, J. Phys. B: At., Mol. Opt. Phys. **40**, 1875 (2007).
[24] R. R. Lucchese, Effects of interchannel coupling on the photoionization cross sections of carbon dioxide, J. Chem. Phys. **92**, 4203 (1990).
[25] G. T. Surratt and W. A. Goddard III, Theoretical studies of $CH_3$, ${CH_3}^+$, and ${CH_3}^-$ using correlated wave functions, Chem. Phys. **23**, 39 (1977).
[26] I. Cacelli, V. Carravetta, and R. Moccia, Photoionisation cross section calculations using Dyson amplitudes: results for Ne, J. Phys. B: At. Mol. Phys. **16**, 1895 (1983).
[27] $B_{LM_L}$'s are generally complex with the restrictions $B^*_{LM_L} = (-1)^{M_L} B_{L-M_L}$ and $|B_{LM_L}|/B_{00} \leqslant \sqrt{2L+1}$ to make $I(\theta,\varphi)$ real and non-negative, respectively. More rigorous inequality for $M_L \neq 0$ is $|B_{LM_L}|/B_{00} \leqslant \sqrt{(2L+1)/2}$. It is derived from $|B_{LM_L}| = |\int I(\theta,\varphi) Y^*_{LM_L}(\theta,\varphi) d\cos\theta\, d\varphi| \leqslant \int \delta(\cos\theta - \cos\theta_{\max})\delta(\varphi - \varphi_{\max})|Y^*_{LM_L}(\theta_{\max},\varphi_{\max})| d\cos\theta\, d\varphi$, where $\theta_{\max}$ and $\varphi_{\max}$ are angles for the maximum $|Y_{LM_L}(\theta,\varphi)|$.
[28] J. S. Griffith, *The Irreducible Tensor Method for Molecular Symmetry Groups* (Dover, New York, 2006).
[29] Y.-I. Suzuki, Direct relation of molecular orbital symmetry with photoelectron angular distributions from aligned molecules in the gas phase, J. Phys. B: At., Mol. Opt. Phys. **41**, 215204 (2008).
[30] Because cyclopropane has the twofold and mirror symmetries, respectively, about the $x$ axis and $xy$ plane, $b^{(\gamma_t q_t, \gamma_t' q_t')}_{KLk_2\Lambda p}$ vanish when $K + p$ or $L + \Lambda$ is odd.
[31] J. R. Appling, M. G. White, R. L. Dubs, S. N. Dixit, and V. McKoy, Circular dichroism in photoelectron angular distributions from two-color (1+1) REMPI of NO, J. Chem. Phys. **87**, 6927 (1987).
[32] M. W. Schmidt, K. K. Baldridge, J. A. Boatz, S. T. Elbert, M. S. Gordon, J. H. Jensen, S. Koseki, N. Matsunaga, K. A. Nguyen, S. J. Su, T. L. Windus, M. Dupis, and J. A. Motogomery, General atomic and molecular electronic structure system, J. Comput. Chem. **14**, 1347 (1993).
[33] D. Dill and J. L. Dehmer, Electron-molecule scattering and molecular photoionization using the multiple-scattering method, J. Chem. Phys. **61**, 692 (1974).
[34] P. Downie and I. Powis, Molecule-frame photoelectron angular distributions from oriented $CF_3$ I molecules, Phys. Rev. Lett. **82**, 2864 (1999).
[35] Y.-I. Suzuki and T. Suzuki, Effect of electron correlation and shape resonance on photoionization from the $S_1$ and $S_2$ states of pyrazine, J. Chem. Phys. **137**, 194314 (2012).
[36] C. Westphal, J. Bansmann, M. Getzlaff, and G. Schönhense, Circular dichroism in the angular distribution of photoelectrons from oriented CO molecules, Phys. Rev. Lett. **63**, 151 (1989).
[37] V. V. Kuznetsov, S. K. Semenov, and N. A. Cherepkov, Photoionization of fixed-in-space molecules by partially polarized light, J. Chem. Phys. **134**, 134301 (2011).
[38] E. Shigemasa, K. Ueda, Y. Sato, T. Sasaki, and A. Yagishita, Symmetry-resolved $K$-shell photoabsorption spectra of free $N_2$ molecules, Phys. Rev. A **45**, 2915 (1992).
[39] R. N. Zare, *Angular Momentum: Understanding Spatial Aspects in Chemistry and Physics* (Wiley, New York, 1988).